

# Open-Narrow-Synechia Anterior Chamber Angle Classification in AS-OCT Sequences

Huaying Hao<sup>1</sup>, Huazhu Fu<sup>2\*</sup>, Yanwu Xu<sup>3</sup>, Jianlong Yang<sup>1</sup>, Fei Li<sup>5</sup>, Xiulan Zhang<sup>5</sup>, Jiang Liu<sup>4</sup>, and Yitian Zhao<sup>1\*</sup>

<sup>1</sup> Cixi Institute of Biomedical Engineering, Ningbo Institute of Materials Technology and Engineering, Chinese Academy of Sciences, Ningbo, China,

yitian.zhao@nimte.ac.cn

<sup>2</sup> Inception Institute of Artificial Intelligence, hzfu@ieee.org

<sup>3</sup> Baidu Inc

<sup>4</sup> Southern University of Science and Technology

<sup>5</sup> State Key Laboratory of Ophthalmology, Zhongshan Ophthalmic Center, Sun Yat-sen University, Guangzhou

**Abstract.** Anterior chamber angle (ACA) classification is a key step in the diagnosis of angle-closure glaucoma in Anterior Segment Optical Coherence Tomography (AS-OCT). Existing automated analysis methods focus on a binary classification system (i.e., open angle or angle-closure) in a 2D AS-OCT slice. However, clinical diagnosis requires a more discriminating ACA three-class system (i.e., open, narrow, or synechia angles) for the benefit of clinicians who seek better to understand the progression of the spectrum of angle-closure glaucoma types. To address this, we propose a novel sequence multi-scale aggregation deep network (SMA-Net) for open-narrow-synechia ACA classification based on an AS-OCT sequence. In our method, a Multi-Scale Discriminative Aggregation (MSDA) block is utilized to learn the multi-scale representations at slice level, while a ConvLSTM is introduced to study the temporal dynamics of these representations at sequence level. Finally, a multi-level loss function is used to combine the slice-based and sequence-based losses. The proposed method is evaluated across two AS-OCT datasets. The experimental results show that the proposed method outperforms existing state-of-the-art methods in applicability, effectiveness, and accuracy. We believe this work to be the first attempt to classify ACAs into open, narrow, or synechia types grading using AS-OCT sequences.

**Keywords:** Angle-closure glaucoma, anterior chamber angles, AS-OCT

## 1 Introduction

Glaucoma is one of the most significant causes of irreversible blinding worldwide, and primary angle-closure glaucoma (PACG) is the major cause of blindness in Asian populations [1]. Anterior Segment Optical Coherence Tomography (AS-OCT) imaging, as a non-contact and non-invasive tool, is widely used to observe

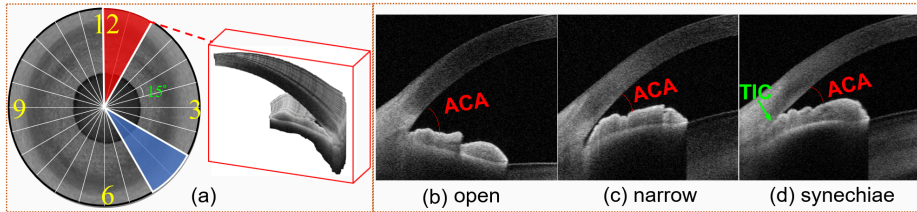


Fig. 1: (a) Visual demonstration of manual annotations by gonioscopy. ACA angles in the 12-1 o'clock region (red) viewed with synechiae, and 4-5 o'clock (blue) viewed with narrow ACAs, and a sequence of AS-OCT images in a random  $15^\circ$  radiant area. (b)-(d) Image samples of open-narrow-synechiae ACA grading.

cross-sections of the anterior segment structure, to assist ophthalmologists in early screening and accurate assessment of PACG [2], as shown in Fig. 1(a).

According to the configuration of the anterior chamber angle (ACA), cases of glaucoma may first be classified into two types: primary open angle glaucoma (Fig. 1(b)); and angle-closure glaucoma (Fig. 1(c-d)). Drawing on epidemiological research [3], clinicians have suggested that angle-closure glaucoma may be further divided into different sub-stages: primary angle closure suspect (PACS), and primary angle-closure/primary angle-closure glaucoma (PAC/PACG). PACS denotes the eye with **narrow** but non-adhesive ACA, as shown in Fig. 1(c), while PAC/PACG denotes the eye with an occludable ACA, *a.k.a.*, **synechiae**, which leads to the presence of trabecular iris contact (TIC) [4], as shown in Fig. 1(d). This secondary level of grading would benefit clinicians in better understanding the progression of the spectrum of angle-closure glaucoma types. Moreover, surgical treatment during PACS can open any non-firm adhesion between the peripheral iris and the trabecular meshwork, which may avoid or alleviate the permanent adhesion seen in the progression to PACG [5]. Therefore, the accurate identification of open-narrow-synechiae ACAs is potentially important in guiding clinical management at different stages of angle-closure glaucoma.

Several methods have been proposed to enable automatic classification of open angle and angle-closure ACAs from AS-OCT images. Xu *et al.* [6, 7] began by localizing the ACA region, and then classified the ACA into open angle or angle-closure based on visual features present in their AS-OCT images. Fu *et al.* [8] proposed a data-driven approach to integrate AS-OCT segmentation, clinical parameter measurements, and glaucoma screening. However, clinical measurement-based methods rely heavily on precise segmentation of the AS-OCT structure. Recently, deep learning-based methods have demonstrated superior performance in ACA classification [2, 9]. Fu *et al.* [4] proposed a multi-context deep network, in which parallel convolutional neural networks are applied to ACA regions and at corresponding scales known to be informative for clinically diagnosing angle-closure glaucoma. Xu *et al.* [9] employed deep learning classifiers for automated detection of gonioscopic angle closure and primary angle closure. However, multi-level network learning is costly in terms of storage

capacity, and slow to proceed to inference. In addition, it depends on a proper integration model, in the absence of which it is less effective than a single model.

All the aforementioned methods focus on the binary classification of open angle and angle-closure in a 2D slice. The open-narrow-synechia ACA classification based on an AS-OCT sequence has been rarely explored, despite its significance in understanding disease progression [10]. Inspired by the procedures of the dynamic gonioscopy examination, in which ophthalmologists move the gonioscope counterclockwise and make an annotation every  $15^\circ$  (see left row of Fig. 1(a)), we address the open-narrow-synechia ACA classification as an image sequence classification problem. The main contributions of this paper are summarized as follows. **(1)** We develop a sequence multi-scale aggregation deep network (SMA-Net) for discriminating the temporal dynamics of features in order to classify ACAs into the open-narrow-synechia grading, using AS-OCT sequences. To best of our knowledge, this is the first work in the area of automated open-narrow-synechia ACA classification. **(2)** A multi-scale discriminative aggregation (MSDA) block is designed to extract the multi-scale representations at slice level, and a ConvLSTM is employed to study the temporal dynamics of these representations at sequence level. **(3)** A new multi-loss function is used to combine slice-based and sequence-based losses, so as to extract spatial and temporal features from AS-OCT sequences. **(4)** Our proposed method outperforms existing state-of-the-art methods in applicability, effectiveness, and accuracy on two AS-OCT datasets (one public and one private dataset).

## 2 Methodology

Fig. 2(a) illustrates the framework of our SMA-Net. Given an AS-OCT sequence, first, a coarse-to-fine method [10] is utilized to localize the ACA regions with sizes of  $448 \times 448$  pixels for each AS-OCT slice, which is the most useful discriminative area for glaucoma classification. Then, a cropped ACA sequence with of size  $224 \times 224 \times T$  is obtained and fed to MSDA blocks to extract a sequence of feature maps at slice level. Here  $T$  denotes the scan number of the AS-OCT within a  $15^\circ$  radiant area. Finally, a stacked 2-layer ConvLSTM is employed to study the temporal dynamics of these representations at sequence level, which produces the prediction of open-narrow-synechia ACA.

### 2.1 Multi-Scale Discriminative Aggregation Block

In our method, each MSDA block consists of a depthwise separable convolutional module and an aggregation gate module. The structure of a depthwise separable convolutional module includes one  $1 \times 1$  convolutional layer and three  $3 \times 3$  atrous convolutional layers, as shown in Fig. 2(b). The separable convolution not only reduces the number of parameters, but improves feature learning ability of the network [11, 12].  $\mathbf{x}$  denotes the output of the  $1 \times 1$  convolution, and  $\mathbf{f}_i$  corresponding to  $3 \times 3$  atrous convolutional layers are used to enlarge the receptive field, with different dilation rates  $i \in \{1, 2, 3\}$ . Moreover, Batch

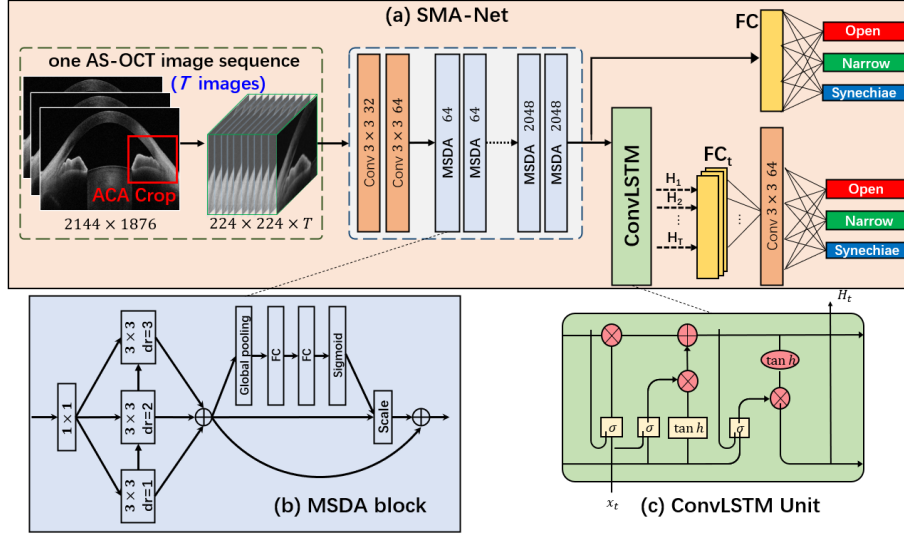


Fig. 2: Overview of our SMA-Net for open-narrow-synechia ACA classification based on an AS-OCT sequence.

Normalization and ReLU activation are used for each convolutional layer. The feature  $\mathbf{x}$  is added to the output of  $\mathbf{f}_{i-1}$ , and then fed into  $\mathbf{f}_i$ , as

$$\mathbf{y}_i = \begin{cases} \mathbf{f}_i(\mathbf{x}), & i = 1 \\ \mathbf{f}_i(\mathbf{x} + \mathbf{y}_{i-1}), & i > 1 \end{cases}, \quad (1)$$

where  $\mathbf{y}_i$  denotes the output of  $\mathbf{f}_i$ . Finally, multi-scale convolutional features are aggregated as the output of the depthwise separable convolutional module. Compared with existing multi-scale blocks, our block effectively reduces the number of parameters within the hierarchical aggregation structure.

In order to combine different scale representations more effectively, an aggregation gate is also introduced, using a Squeeze and Excitation (SE) module to obtain discriminative representation. With the output of the depthwise separable convolutional module, the SE module is used in our block followed the coarse fusion to the new output. More specifically, the SE module is composed of a global average pooling layer and a Multi-Layer Perceptron (MLP) with a ReLU-activated hidden layer, followed by the sigmoid activation. Note that the SE module follows a self-attention architecture, which can selectively enhance discriminative representation. In contrast to single feature addition fusion, this more discriminative fusion can achieve dynamic weighted distribution in the channels of multi-scale branches.

## 2.2 Open-narrow-synechia ACA classification

In our method, Xception architecture [11] is used as the backbone. We replace the  $3 \times 3$  convolution with our MSDA block, which can learn multi-scale repre-

sentation and integrate the discriminative representation with the output. With the slice-based features from MSDA blocks, a stacked 2-layer ConvLSTM, with 1024 hidden units in each of the cells, is used to process feature maps and generate a sequence of ConvLSTM states  $\{\mathbf{H}_1, \mathbf{H}_2, \dots, \mathbf{H}_T\}$ , which can learn spatial and temporal information by spatial dependencies, as shown in Fig. 2(c). At each position  $t$ , the output state  $\mathbf{H}_t$  is fed into a global average pooling and a fully connected (FC) layer that computes the estimated probabilities  $\{\mathbf{Y}_1, \mathbf{Y}_2, \dots, \mathbf{Y}_T\}$ .

In this work, we consider a multi-level loss function to combine slice-based and sequence-based losses. To optimize the SMA-Net and avoid gradient disappearance, we propose to use cross entropy loss as our slice-based loss. To be specific, we use global average pooling and an FC layer to generate estimated probabilities  $\mathbf{Y}_t^s$  from each slice  $t$ . To this end, the slice-based loss is defined as:

$$\mathcal{L}_{2D} = \sum_{t=1}^T \{\mathcal{L}_{CE}(\mathbf{Y}_t^s, \mathbf{Y}^*)\}, \quad (2)$$

where  $\mathcal{L}_{CE}$  represents cross entropy loss, and  $\mathbf{Y}^*$  denotes the ground truth of the input AS-OCT sequence. Note that in our method, all AS-OCT slices have the same labels within the whole sequence.

To improve performance, we use a weighted ensemble (WE) method to optimize the final result by these estimated probabilities. We first concatenate a sequence of estimated probabilities to obtain a new descriptor with dimension  $T \times 3$ . We then perform a 1-D convolution operation with on the new descriptor, and feed the result to the FC layer for final classification  $\mathbf{Y}_f$ , which can weight predictions of  $T$  state. Finally, we define a new loss-based cross entropy as our sequence-based loss function:

$$\mathcal{L}_{3D} = \sum_{i=1}^t \{\mathcal{L}_{CE}(\mathbf{Y}_i, \mathbf{Y}^*)\}. \quad (3)$$

Therefore, the overall loss function of our network is as:

$$\mathcal{L}_{SV} = \mathcal{L}_{2D} + \lambda \mathcal{L}_{3D}, \quad (4)$$

where  $\lambda$  is the balance weight ( $\lambda = 1$  in our experiment).

### 3 Experimental Results

The proposed architecture was implemented using the publicly available Pytorch Library. In the training phase, we employed an Adam optimizer to optimize the deep model. We used a gradually decreasing learning rate, starting from 0.0001. In addition, online data enhancement was employed to enlarge the training data, which includes brightness, color, contrast and sharpness transformations, and we set a random seed from 1 to 4 for enhancement.

Table 1: Classification of the open-narrow-synechiaes ACAs by different methods on the private dataset.

Methods	$kappa$	$F1$	$B-Acc$	$Sen$	$Spe$
ResNet-34 [13]	0.6766	0.7527	0.8188	0.7485	0.8891
MSCNN [10]	0.6773	0.7498	0.8171	0.7455	0.8887
Xception [11]	0.7252	0.7835	0.8393	0.7752	0.9035
MA-Net	0.7477	0.8121	0.8600	0.8063	0.9137
C3D [14]	0.7489	0.8115	0.8532	0.8048	0.9136
I3D [15]	0.7662	0.8171	0.8619	0.8073	0.9166
S3D [16]	0.7431	0.8007	0.8567	0.8016	0.9119
Our SMA-Net	<b>0.7931</b>	<b>0.8459</b>	<b>0.8829</b>	<b>0.8371</b>	<b>0.9282</b>

### 3.1 Performance of open-narrow-synechiaes ACA classification

**Private dataset:** All AS-OCT volumes in our dataset were captured by a CASIA-2 machine (Tomey Inc., Japan) from 66 eyes with open-narrow-synechiaes grading (human expert annotations of images derived from by dynamic gonioscopic examinations). Each volume contains 128 AS-OCT images, and each slice in a volume is  $2144 \times 1876$  pixels. A senior ophthalmologist annotated each  $15^\circ$  segment of the ACAs of an eye, yielding 24 annotations for each single eye, and resulting in a total of 1584 annotations for this dataset. In light of this, we formed the AS-OCT slices ( $T = 11$  slices) in each  $15^\circ$  region as one sequence. Finally, a total of 1584 image sequences are generated, in which 504 sequences are annotated with open ACA, 742 sequences are with narrow ACA, and 338 sequences contain synechiaes ACA. In our experiments, the dataset was equally and randomly divided into training and testing sets, taking into account the integrity of data from each eye, so that two ACAs from the same eye would not be separated between the training and testing sets.

In order to demonstrate the superiority of the proposed method for classification of open-narrow-synechiaes angle, we carry out a comprehensive comparison between the proposed method and the following state-of-the-art methods: (1) 2D deep models: Multi-Scale Regions Convolutional Neural Networks (MSCNN) [10]; Resnet-34 [13]; Xception [11]; and MA-Net (Xception with our MSDA block). 3D deep models: C3D [14]; I3D [15]; and S3D [16]. Following the standard performance assessment protocol for multi-class classification [17], we use weighted sensitivity ( $Sen$ ), specificity ( $Spe$ ), and balanced accuracy ( $B-acc$ ). In order to reflect the trade-offs between  $Sen$  and  $Spe$  and evaluate the quality of our classification results, the  $kappa$  analysis [18] and  $F1$  [19] score were also provided. Table 1 reports the classification performance of different methods. It may be observed that our SMA-Net yields best performance in terms of all metrics when compared to either 2D or 3D deep learning-based methods. The probable reason for this is that the proposed networks can learn rich and discriminative representation from both local features (2D image features) and global geometry (image sequence).

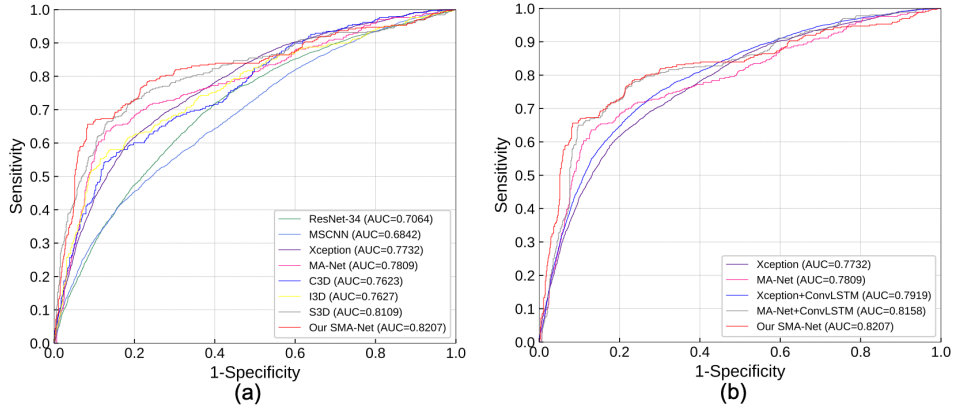


Fig. 3: AUC curves of different approaches in classifying narrow, and synechiae ACA. (a) Comparison of state-of-the-art 2D and 3D deep networks. (b) Ablation study of our model.

Because binary open angle and angle-closure classification is a relatively straightforward and easy task, our method and other networks achieve similar high performances ( $AUC=0.998$ ). Therefore, only the AUC curves in distinguishing narrow and synechiae angles are illustrated in Fig. 3(a). As expected, our method still produced the best performance on the classification of narrow and synechiae angles, with  $AUC=0.8207$ . Overall, all 3D networks achieved relatively higher performances than 2D networks, since a 3D deep network can learn spatial representation from an image sequence.

To evaluate the effectiveness of each module in our network, we provide an ablation study, and the results are reported in Table 2 and Fig. 3(b). Results show that the Xception+ConvLSTM and MA-Net+ConvLSTM method clearly outperformed the and Xception and MA-Net alone, with improvement of about 4.53% and 3.43% in  $kappa$ , and about 1.87% and 3.49% in AUC. This demonstrates that the ConvLSTM learns discriminative representations from an AS-OCT image sequence, and is capable of preserving the spatial information, so memorizing the change in appearance that corresponds to motion information (neighboring slices), thereby improving performance in separating narrow angle and fully closed angle. Table 2 and Fig. 3(b) also reveal that after  $\mathcal{L}_{SV}$  was applied, classification performance of our SMA-Net (MA-Net+ConvLSTM+ $\mathcal{L}_{SV}$ ) improved significantly, with an improvement of approximately 4.53% in  $kappa$  and 0.49% in AUC, respectively. This is because with  $\mathcal{L}_{SV}$ , the ConvLSTM explores the temporal dynamics of appearance features of an AS-OCT sequence, and these features are further aggregated for classification purposes.

### 3.2 Performance of open angle and angle-closure classification

We also evaluated our method for binary ACA classification, i.e., open angle and angle-closure cases. The public AS-OCT dataset, Angle-closure Glaucoma

Table 2: Classification performance of the open-narrow-synechia ACAs by different module combinations on private dataset.

Methods	$\kappa$	$F1$	$B\text{-acc}$	$Sen$	$Spe$
Xception [11]	0.7252	0.7835	0.8393	0.7752	0.9035
MA-Net	0.7477	0.8121	0.8600	0.8063	0.9137
Xception+ConvLSTM	0.7705	0.8238	0.8664	0.8135	0.9194
MA-Net+ConvLSTM	0.7820	0.8377	0.8780	0.8310	0.9250
MA-Net+ConvLSTM+ $\mathcal{L}_{SV}$	<b>0.7931</b>	<b>0.8459</b>	<b>0.8826</b>	<b>0.8371</b>	<b>0.9282</b>

Table 3: Performance of compared methods on AGE dataset.

Methods	AUC	$Sen$	$Spe$
Resnet-34 [13]	0.990959	0.859375	0.999219
Inception-V3 [20]	0.999285	0.918750	0.998438
Xception [11]	0.999347	0.950000	0.996094
MCDN [21]	0.999604	0.959375	0.998438
MSCNN [10]	0.999727	0.978125	0.996875
SMA-Net	<b>1.000000</b>	<b>1.000000</b>	<b>1.000000</b>

Evaluation (AGE) dataset [22] was used, which includes 3200 AS-OCT images with resolution of  $2130 \times 998$  pixels. These images were divided into two sets: 1600 training and 1600 testing.

In this experiment, we changed the output of our method to binary classification. We carried out a comprehensive comparison between the proposed and the state-of-the-art methods: Multi-Context Deep Network (MCDN) [21], Multi-Scale Regions Convolutional Neural Networks (MSCNN) [10]; Resnet-34 [13]; Inception-V3 [20]; and Xception [11]. Table 3 shows that our SMA-Net outperforms all competing methods in terms of all metrics (AUC,  $Sen$  and  $Spe$ ). To be more specific, it can be seen that our SMA-Net outperforms the Xception (our backbone network) alone, with improvement of 5.00% in  $Sen$ . Interestingly, all the methods achieved remarkable AUC scores. This is because, as we suggested above, the binary classification of open or angle-closure is relatively easy, and this finding is also evidenced by the leader board of AGE challenge - the task of open angle and angle-closure classification by means of AS-OCT has attained remarkably high standards of performance by using state-of-the-art deep networks, with AUC scores higher than 0.98 across the board. Another reason is that AGE dataset was motivated for the classification of explicit open and closed ACA.

## 4 Conclusion

Most of the existing automated methods are only able to classify the ACA as either open or angle-closure. In this paper, we proposed an automated ACA classification framework, which is not only able to classify open angle and angle-closure, but is also capable of grading the three-class open-narrow-synechia



ACA from AS-OCT imagery, so as to further guide clinical management at different stages of glaucoma. To be more specific, we introduced a novel block, named the MSDA block, with a view to learning multi-scale discriminative representations over AS-OCT volumes. In addition, a new multi-loss function is used to combine the slice-based and sequence-based losses, as thus to extract spatial and temporal features from AS-OCT image sequences. The results demonstrate that the proposed method outperforms other state-of-the-art 2D and 3D deep networks. It may be expected that the proposed model could be a powerful tool for diagnosing the presence, and analyzing the progression of angle-closure glaucoma.

## References

1. Tham, Y.C., Li, X., Wong, T.Y., Quigley, H.A., Aung, T., Cheng, C.Y.: Global prevalence of glaucoma and projections of glaucoma burden through 2040: a systematic review and meta-analysis. *Ophthalmology* **121**(11) (2014) 2081–2090
2. Fu, H., Baskaran, M., Xu, Y., Lin, S., Wong, D.W.K., Liu, J., Tun, T.A., Mahesh, M., Perera, S.A., Aung, T.: A deep learning system for automated angle-closure detection in anterior segment optical coherence tomography images. *American journal of ophthalmology* **203** (2019) 37–45
3. Foster, P.J., Buhrmann, R., Quigley, H.A., Johnson, G.J.: The definition and classification of glaucoma in prevalence surveys. *British journal of ophthalmology* **86**(2) (2002) 238–242
4. Fu, H., Xu, Y., Lin, S., Wong, D.W.K., Baskaran, M., Mahesh, M., Aung, T., Liu, J.: Angle-closure detection in anterior segment oct based on multilevel deep network. *IEEE Transactions on Cybernetics* (2019)
5. Shang, Q., Zhao, Y., Chen, Z., Hao, H., Li, F., Zhang, X., Liu, J.: Automated iris segmentation from anterior segment oct images with occludable angles via local phase tensor. In: *EMBC, IEEE* (2019) 4745–4749
6. Xu, Y., Liu, J., Tan, N.M., Lee, B.H., Wong, D.W.K., Baskaran, M., Perera, S.a., Aung, T., Tin, A.: Anterior chamber angle classification using multiscale histograms of oriented gradients for glaucoma subtype identification. In: *EMBC, IEEE* (2012) 3167–3170
7. Xu, Y., Liu, J., Cheng, J., Lee, B.H., Wong, D.W.K., Baskaran, M., Perera, S., Aung, T.: Automated anterior chamber angle localization and glaucoma type classification in oct images. In: *EMBC, IEEE* (2013) 7380–7383
8. Fu, H., Xu, Y., Lin, S., Zhang, X., Wong, D.W.K., Liu, J., Frangi, A.F., Baskaran, M., Aung, T.: Segmentation and quantification for angle-closure glaucoma assessment in anterior segment oct. *IEEE Transactions on Medical Imaging* **36**(9) (2017) 1930–1938
9. Xu, B.Y., Chiang, M., Chaudhary, S., Kulkarni, S., Pardeshi, A.A., Varma, R.: Deep learning classifiers for automated detection of gonioscopic angle closure based on anterior segment oct images. *American journal of ophthalmology* (2019)
10. Hao, H., Zhao, Y., Fu, H., Shang, Q., Li, F., Zhang, X., Liu, J.: Anterior chamber angles classification in anterior segment oct images via multi-scale regions convolutional neural networks. In: *EMBC, IEEE* (2019) 849–852
11. Chollet, F.: Xception: Deep learning with depthwise separable convolutions. In: *CVPR, IEEE* (2017) 1251–1258

12. Yu, F., Wang, D., Shelhamer, E., Darrell, T.: Deep layer aggregation. In: CVPR, IEEE (2018) 2403–2412
13. He, K., Zhang, X., Ren, S., Sun, J.: Deep residual learning for image recognition. In: CVPR, IEEE (2016) 770–778
14. Tran, D., Bourdev, L., Fergus, R., Torresani, L., Paluri, M.: Learning spatiotemporal features with 3d convolutional networks. In: CVPR, IEEE (2015) 4489–4497
15. Carreira, J., Zisserman, A.: Quo vadis, action recognition? a new model and the kinetics dataset. In: CVPR, IEEE (2017) 6299–6308
16. Xie, S., Sun, C., Huang, J., Tu, Z., Murphy, K.: Rethinking spatiotemporal feature learning: Speed-accuracy trade-offs in video classification. In: ECCV, Springer (2018) 305–321
17. Annunziata, R., Kheirkhah, A., Aggarwal, S., Hamrah, P., Trucco, E.: A fully automated tortuosity quantification system with application to corneal nerve fibres in confocal microscopy images. *Med. Image Anal.* **32** (2016) 216–232
18. [https://en.wikipedia.org/wiki/Cohen%27s\\_kappa/](https://en.wikipedia.org/wiki/Cohen%27s_kappa/)
19. [https://en.wikipedia.org/wiki/F1\\_score/](https://en.wikipedia.org/wiki/F1_score/)
20. Xia, X., Xu, C., Nan, B.: Inception-v3 for flower classification. In: ICIVC, IEEE (2017) 783–787
21. Fu, H., Xu, Y., Lin, S., Wong, D., Mani, B., Mahesh, M., Aung, T., Liu, J.: Multi-context deep network for angle-closure glaucoma screening in anterior segment oct. In: MICCAI, Springer (2018) 356–363
22. Fu, H., Li, F., Sun, X., et al.: AGE Challenge: Angle Closure Glaucoma Evaluation in Anterior Segment Optical Coherence Tomography. arXiv (2020)